Turkish Journal of Electrical Engineering & Computer Sciences

http://journals.tubitak.gov.tr/elektrik/

Research Article

Turk J Elec Eng & Comp Sci
(2015) 23: 395 – 420

doi:10.3906/elk-1212-31

# Hybrid adaptive neuro-fuzzy B-spline–based SSSC damping control paradigm using online system identification

**Laiq KHAN, Rabiah BADAR***
Department of Electrical Engineering, COMSATS Institute of Information Technology, Abbottabad, Pakistan

**Received:** 05.12.2012 • **Accepted:** 05.03.2013 • **Published Online:** 23.02.2015 • **Printed:** 20.03.2015

**Abstract:** B-spline membership functions have produced promising results in the field of signal processing and control due to their local control property. This work explores the potential of B-spline–based adaptive neuro-fuzzy wavelet control to damp low frequency power system oscillations using a static synchronous series compensator (SSSC). A comparison of direct and indirect adaptive control based on hybrid adaptive B-spline wavelet control (ABSWC) is presented by introducing the online identification block. ABSWC with identification (ABSWCI) provides the sensitivity information of the plant needed to control the system. The parameters of the control and identification block are updated online using a gradient descent-based backpropagation algorithm. The stability and convergence of the proposed control system is discussed based on Lyapunov stability criteria. The robustness of the proposed control algorithm has been evaluated for local and interarea modes of oscillations using different faults. The nonlinear time-domain simulations have been analyzed on the basis of different performance indices and time-frequency representation, showing that ABSWC effectively damps low-frequency oscillations and incorporation of online identification optimizes the control system performance in terms of control effort, which reduces the switching losses of the converter.

**Key words:** Adaptive neuro-fuzzy, SSSC multimachine system, B-spline, wavelets

## 1. Introduction

The demand for continuous and good-quality power supplies for large infrastructures, like communication and transportation systems, in addition to the consumption of electricity for daily life, highlights the importance of stable, secure, and reliable operation of power systems. The geographical enhancements and technological advancement of power-consuming systems demand the structural expansion of power systems and power transmission over long distances. However, the structural expansion of existing power systems is restricted due to environmental and economic factors, making the systems operate close to their maximum limits; hence, the systems work in highly stressed conditions. In the case of a fault event such as loss of load or generating unit, 3-phase to ground fault, etc., transient stability can become a transmission limiting factor due to the increased loading of long transmission lines [1].

Transient stability is the stability associated with rotor angle oscillations. Power system stability can be defined as the system's ability to regain its state of equilibrium after the occurrence of a physical disturbance. Transient stability is the ability of the power system to maintain its synchronism when subjected to large disturbances [2]. In the steady state, all the generating units connected in a large power system operate at the same speed, known as synchronous speed. However, a speed imbalance occurs when the steady state of

*Correspondence: rabiahbadar@ciit.net.pk

the system is disrupted. This may cause a machine or group of machines to accelerate in one area of a power network and decelerate in another, resulting in low-frequency electromechanical oscillations (LFEMOs) [3–5].

These LFEMOs, arising due to lack of damping torque, are a consistent threat to the stable operation of a power system, as they may grow indefinitely if not damped out properly, which eventually leads to partial or full system outage. Major blackouts have been reported in the literature due to these LFEMOs [6]. The installation of automatic voltage regulators (AVRs) and power system stabilizers (PSSs) is a cost-effective remedy to restore system stability [7–10]. However, these devices are simple and linear in nature and are locally installed in generating units, thus exhibiting poor damping performance due to lack of information about the global behavior of the system.

In their quest for secure power transmission over long distances while avoiding the expansion of existing systems, researchers have found that the power flow on a line can be controlled by changing voltage phase, magnitude, and impedance of the transmission line, which eventually led to the emergence of the flexible AC transmission system (FACTS). The concept of FACTS was first proposed by Gyuayi and Hingorani in the 1980s [11].

The static synchronous series compensator (SSSC) is a second-generation series FACTS controller that was proposed by Gyugyi in 1989 [12]. Due to its superior performance over other series FACTS controllers and its simplicity of control, the SSSC has been widely discussed in the literature [13–17]. Controlling power flow on a line and improving power system stability using SSSCs was discussed in [18–20].

The primary goal of the SSSC is not to damp the power system oscillations, but rather to control the power flow online. The additional feature of damping LFEMOs can be exploited by installing an auxiliary damping control with the SSSC. The performance of the SSSC in damping power system oscillations depends upon the control system design.

In the literature, many control techniques ranging from linear to nonlinear, conventional to adaptive, and metaheuristic to Neuro-Fuzzy, and their hybrids, have been proposed for power system damping control using SSSC.

In [21], the linearized Phillips–Heffron model and single input/single output (SISO) control structure were used to propose the damping function of the SSSC. A nonlinear controller based on Lyapunov's stability criterion was designed to improve the stability region and damping performance for a single machine infinite bus (SMIB) system using the SSSC [22]. Linear control techniques are not suitable for highly nonlinear plants like power systems and may perform better only in the vicinity of the operating point for which the controller was designed. On the other hand, nonlinear control techniques need the exact mathematical information of the plant.

Proportional integral (PI) and proportional derivative (PD) controllers with gain adjustment based on different optimization techniques, like particle swarm optimization (PSO), differential evolution (DE) [23], and genetic algorithms (GAs), are widely used for SSSC control to damp power system oscillations. Swain et al. proposed a method based on a real coded GA for tuning the controller parameters [24]. The robustness of the proposed controller was checked only for the SMIB system. Ajami et al. proposed a multiobjective particle swarm optimization (PSO)-based damping control for SSSCs [25]. The effectiveness of the controller was evaluated using eigenvalue analysis for the SMIB system only. PSO-based neural network (NN) control for SSSCs was proposed in [26], which gives better performance but at the cost of complexity. Panda used PSO, GAs, and their variants for optimal tuning of parameters of lead-lag controllers to improve the damping capability of SSSCs [27–30]. An adaptive fuzzy control of the SSSC for damping power system oscillations

was presented in [31]. The parameters of the controller were identified online by using the recursive least square (RLS) algorithm, but the control system was tested for the SMIB system. A detailed review of different soft-computing techniques used to control the operation of different FACTS controllers was presented in [32].

A power system has a highly nonlinear and nonstationary nature. Therefore, the control system must be nonlinear, adaptive, and fast enough to update its parameters with variations in plant dynamics. Metaheuristic techniques are approximate and nondeterministic in nature; moreover, their computational complexity does not encourage their application to large power systems.

Design and structural complexity, vulnerability to changes in operating condition and sensitivity to system model accuracy, computational cost, memory requirements, and latency due to offline training are some of the major shortcomings in these existing control paradigms.

Neuro-fuzzy control structures have found extensive applications in the field of identification and control of nonlinear plants due to their good generalization capability, low complexity, and ease of implementation. A neuro-fuzzy supplementary damping control for multimachine systems was proposed in [33–35]. It utilizes the linearized model of the power system and the manual tuning process for fuzzy control rules, which is an experience-oriented and time-consuming practice. Chandrakar and Kothari investigated the neuro-fuzzy control for transient stability enhancement and improvement in power transfer capability using SSSCs [36].

NNs are well known for their ability to cope with model inaccuracy, good approximation capabilities, and parallel structure, but they suffer from computational burden due to the increase in number of neurons as the dimensions of the problem increase. On the other hand, fuzzy systems are good in dealing with nonlinear systems that have uncertainties; however, their performance depends upon the accuracy of the knowledge base, which in some cases may be difficult to ensure. Therefore, the low computational complexity and knowledge base capability of a fuzzy system was combined with the good generalization properties of NNs into a single structure, known as neuro-fuzzy. However, the system suffers from the inherent drawback of getting stuck in local minima of the search space and poor convergence speed. Moreover, the linear consequent part of conventional fuzzy Takagi–Sugeno–Kang (TSK) systems cannot cope with nonlinearities in the system.

To overcome these limitations of neuro-fuzzy systems, wavelets were introduced into their structure. Wavelet NNs utilize the multiresolution property of wavelets to analyze the local details of the signal and model the system behavior with greater accuracy. Fuzzy wavelet NNs (FWNNs) have been successfully used to control dynamic plants and prediction of time series [37,38]. The wavelet is a function having finite support with most of the energy concentrated in the vicinity of the center. The combination of shifted and translated versions of the mother wavelet can be used to cover the input data space for modeling. However, these controllers have a feed-forward structure and may have losses in their performance for certain dynamic plants, like power systems, due to the globally tuned membership functions in the antecedent part. The shape of the membership function significantly affects the performance of the control system [39–43]. The local control of the membership function enables it to translate the system's uncertainties in the rule base of the fuzzy control.

Curry and Schoenberg were the first to introduce the theory of B-spline approximation, which was later further worked out by others [44]. B-spline membership functions are locally controllable membership functions and are well known for generating smooth control output. It has been shown that B-spline–based fuzzy NNs have fast convergence as compared to conventional adaptive neuro-fuzzy systems [45]. Due to their local control property, simplicity of implementation, and low computational and storage requirements, they have proven to be a good choice for identification and control of nonlinear systems [46–49]. However, they have been used

in conventional TSK structures with linear or singleton consequent parts, and their combination with more sophisticated techniques like wavelet NNs is still unexplored.

In this work, an adaptive online control system is proposed by optimizing the conventional structure of the TSK fuzzy system. The proposed system utilizes the locally controllable B-spline membership function in the antecedent part of the controller and wavelet functions in the consequent part, with adaptively changing translation and dilation factors, which help to improve the computational strength and generalization capability of the proposed control system. The performance of the proposed network has been investigated using direct and indirect control schemes for damping power system oscillations with smooth control effort. The proposed control scheme synergistically integrates the locally tunable B-spline membership functions of order 2 and time-frequency localization property of Morlet wavelets in the neuro-fuzzy structure. The B-spline functions of order 2 correspond to the locally tunable triangular membership functions, which have a normalization property ensuring the transparency of the neuro-fuzzy network. The performance of the proposed scheme is evaluated using different performance indices. To get clear insight into the behavior of different frequencies, a time-frequency representation method known as smooth pseudo-Wigner–Ville distribution (SPWVD) is used to analyze different modes of oscillations and the control effort.

The rest of the paper is arranged as follows: Section 2 gives the dynamic modeling of SSSC. Section 3 presents the detailed mathematical treatment of control system design. Update laws for parameters adaptation are discussed in Section 4. The proposed online algorithm is presented in Section 5. The stability analysis of the proposed control scheme is given in Section 6. The simulation results are presented in Section 7. Section 8 concludes this research; finally, Section 9 explores the future dimensions of this work.

## 2. SSSC operation, dynamic modeling, and control

The nonlinear dynamic model of a multimachine power system can be written in the form of differentio-algebraic equations as follows:

$$\dot{\mathbf{x}} = f(\mathbf{x}, \mathbf{y}, t), \tag{1}$$

$$\mathbf{0} = g(\mathbf{x}, \mathbf{y}, t), \tag{2}$$

where $\mathbf{x}$is the state variable matrix and $\mathbf{y}$ is the output algebraic variable matrix. The machine and control dynamics are described in the form of differential equations, whereas the algebraic equations comprise load flow and other network equations.

The SSSC is the series compensating controller and consists of 3 main parts: the voltage sourced inverter, the DC capacitor, and the series step-down coupling transformer. The SSSC injects a series of AC voltage in quadrature with the transmission line current at fundamental frequency. Depending upon the demand of the AC network, the SSSC controls the active power flow by working in capacitive or inductive mode. If the voltage injected by the SSSC is negative, it works in inductive mode, whereas in capacitive mode the voltage injection will be positive. In capacitive mode, the injected voltage leads the line current, whereas in inductive mode injected voltage lags the line current. The DC voltage across the capacitor is maintained at a constant level by drawing a small amount of active power from the AC network to compensate for the converter losses.

Figure 1 shows the complete diagram of the AC power system. SSSC is installed on a transmission line between nodes 1 and 2. In the power system, SSSC can be modeled as series voltage source and reactance. By approximating the switching functions with their fundamental frequency components, SSSC converter output can be modeled by transforming the 3-$\varphi$ voltages and currents to $dq$ variables [50]. The converter output

voltage is given by:

$$\begin{pmatrix} v_{d\_inv} \\ v_{q\_inv} \end{pmatrix} = \begin{pmatrix} v_1 \cos\psi_s \\ v_1 \sin\psi_s \end{pmatrix}, \tag{3}$$

where $\psi_s = \theta + \phi$ is the converter output voltage angle and $v_1 = mkv_{DC}$. Here, $\phi$ is the firing angle, $m$ is the modulation index, and $k$ is a constant defining the relationship between converter AC and DC side voltages.

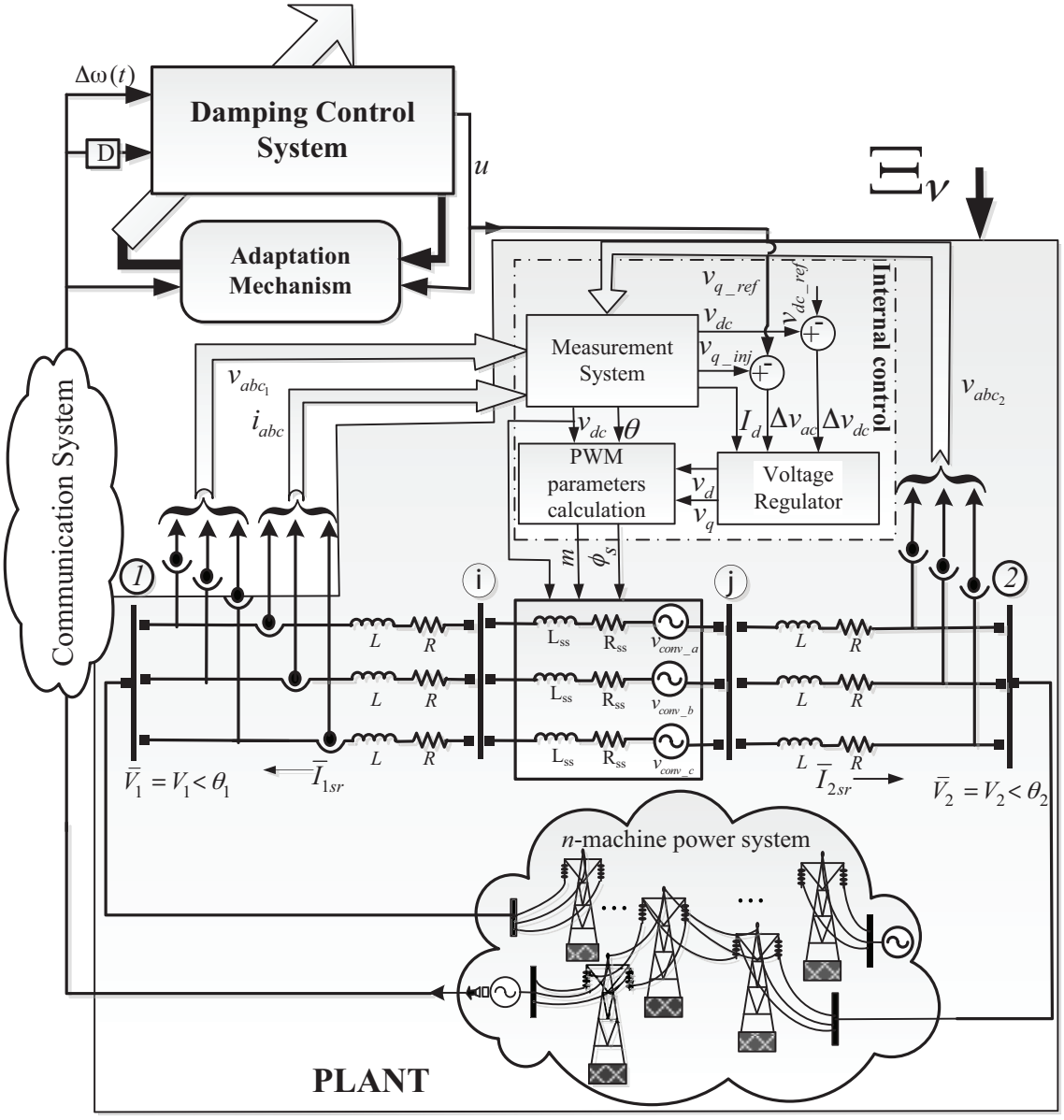


**Figure 1.** Power system model installed with SSSC.

The DC side voltage can be calculated using the law of power conservation and is given as:

$$\frac{dv_{DC}}{dt} = \frac{3mk}{2C}\left[i_d \cos\psi_s + i_q \sin\psi_s\right] - \frac{v_{DC}}{C\mathrm{R}_{DC}}. \tag{4}$$

Let $I\angle\theta$ be the current flowing through line in phasor form, with $\theta$ being the angle of line current; then the converter output voltage in phasor form is given by:

$$\bar{V}_{inv} = mkv_{DC}\angle\psi_s. \tag{5}$$

The mathematical model of the 3-$\varphi$ SSSC embedded into the transmission line is given as:

$$\dot{\mathbf{i}}_{abc} = -\frac{R_{ss}}{L_{ss}} I_{3\times3}\mathbf{i}_{abc} + \frac{1}{L_{ss}} I_{3\times3}\left(\mathbf{v}_{abc\_12} - \mathbf{v}_{abc\_inv}\right), \tag{6}$$

where $R_{ss}$ and $L_{ss}$ are the series resistance and inductance of the SSSC including the effects of magnetic coupling and interface transformer, $\mathbf{i}_{abc}$ is the 3-$\varphi$ current matrix, $\mathbf{v}_{abc\_12} = \mathbf{v}_{abc\_1} - \mathbf{v}_{abc\_2}$ is the 3-$\varphi$ voltage matrix based on the voltage difference of the 2 ends, and $\mathbf{v}_{abc\_inv}$ is the 3-$\varphi$ converter output voltage. By applying the $dq$ transformation, Eq. (6) becomes:

$$\begin{pmatrix} \dot{i}_d \\ \dot{i}_q \end{pmatrix} = \begin{pmatrix} -\frac{R_{ss}}{L_{ss}} & -\omega \\ \omega & -\frac{R_{ss}}{L_{ss}} \end{pmatrix} \begin{pmatrix} i_d \\ i_q \end{pmatrix} + \begin{pmatrix} \frac{1}{L_{ss}} & 0 \\ 0 & \frac{1}{L_{ss}} \end{pmatrix} \begin{pmatrix} v_{d\_ij} - v_{d\_inv} \\ v_{q\_ij} - v_{q\_inv} \end{pmatrix}. \tag{7}$$

Combining Eqs. (3), (4), and (7), the complete model can be written as:

$$\begin{pmatrix} \dot{i}_d \\ \dot{i}_q \\ \dot{v}_{\mathrm{DC}} \end{pmatrix} = \begin{pmatrix} -\frac{R_{ss}}{L_{ss}} & -\omega & -\upsilon_3\cos\psi_s \\ \omega & -\frac{R_{ss}}{L_{ss}} & -\upsilon_3\sin\psi_s \\ \upsilon_2\cos\psi_s & \upsilon_2\sin\psi_s & -\frac{1}{CR_{DC}} \end{pmatrix} \begin{pmatrix} i_d \\ iq \\ v_{\mathrm{DC}} \end{pmatrix} + \begin{pmatrix} \frac{1}{L_{ss}} & 0 & 0 \\ 0 & \frac{1}{L_{ss}} & 0 \\ 0 & 0 & \frac{1}{L_{ss}} \end{pmatrix} \begin{pmatrix} v_{d\_ij} \\ v_{q\_ij} \\ 0 \end{pmatrix}, \tag{8}$$

where $\upsilon_2 = \frac{3}{2C}mk$ and $\upsilon_3 = \frac{mk}{L_{ss}}$. The control of SSSC can be categorized as internal and external control. The internal control keeps the injected voltage in quadrature with the line current maintaining the DC voltage at a constant level in steady state. The external control monitors the changes in system variables and provides the reference values to internal control. The internal control block, shown in Figure 1, has 3 main parts. These include the measurement system block, the AC and DC voltage regulators, and the pulse width modulation (PWM) parameters' calculation block. The potential and current transformers sense the 3-phase line voltages and currents, respectively, and input them into the measurement system. The measurement system includes the phase-locked loop (PLL), whose primary goal is to extract the synchronization angle to transform the 3-phase input quantities into $dq$-reference frame.

The quadrature-injected voltage control is carried out using the AC voltage regulator in the voltage regulator block. The converter injected voltage is calculated by the difference of quadrature components of both end voltages of the SSSC and then compared with the reference value. The calculated error is fed to the PI control to generate the desired quadrature voltage component. The direct component of converter voltage is computed by the PI regulator, whose input is the error between reference and measured DC voltages. The gains of the PI controllers are adjusted based on a trial-and-error method. The outputs of the 2 PI controllers are used to calculate modulation index and firing angle using the PWM parameters' calculation block.

The dynamic model of the SSSC is interfaced with other dynamic components of the power system, like synchronous machines, exciters, and controls.

## 3. Control system design

The proposed control scheme is online adaptive, and the inclusion of the identification block makes it indirect. The identification block is used to provide the sensitivity term to the control block to ensure the stability of the system. The plant includes a power system installed with the SSSC. $\Xi_\kappa$ is the set of small and large disturbances applied to the system. The closed-loop structure of the system is shown in Figure 2.

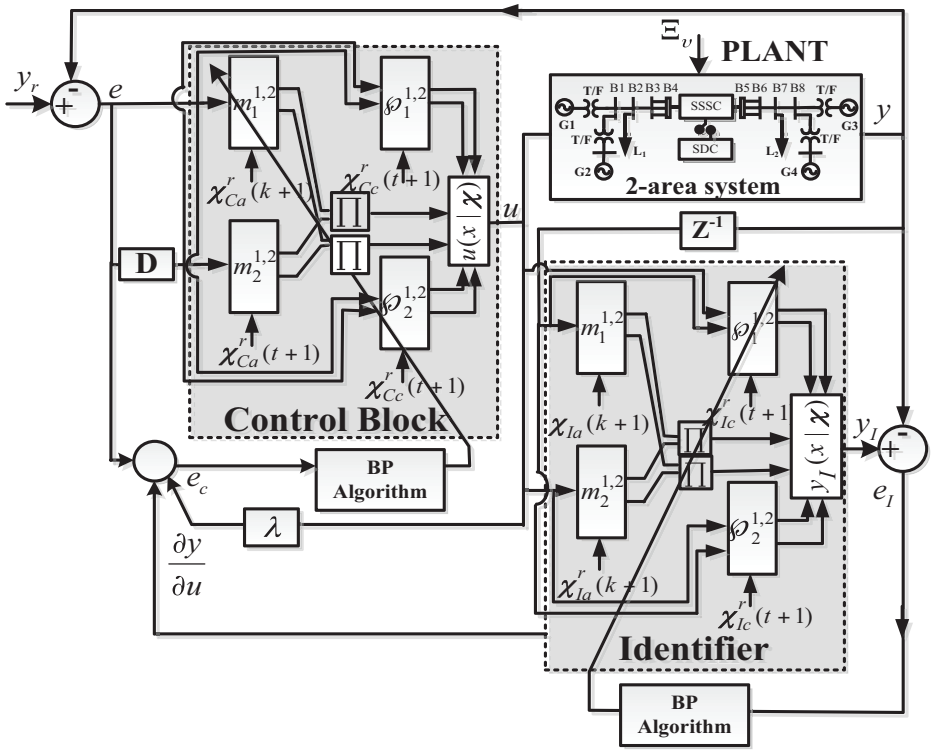


**Figure 2.** Closed-loop control system structure.

The control and identification blocks are based on an adaptive neuro-fuzzy structure defined by the following generalized rule:

$$\Re_j : IF x_1 \text{ is } m_{1j} \text{ and } x_2 \text{ is } m_{2j} \cdots x_{mj} \text{ is } m_{mj} THEN y_j \text{ is } \wp_j.$$

Here, $\Re_j$ is the $j$th rule. *IF* and *THEN* represent the antecedent and consequent parts, respectively. $x_{ij}$ is the $i$th input to $j$th rule, and $m_{ij}$ is the $j$th membership function of the $i$th input. $y_j$ is the output of the consequent part of the $j$th rule, i.e. the output of the wavelet neural network, and is denoted by $\wp_j$.

Both the control and identification block have the same architecture as shown in Figure 3; however, they differ in fuzzification approach to avoid computational complexity and ensure simplicity of implementation. The whole network works in a layered fashion.

**Layer 1** is the input layer, which routes the inputs to the second layer for fuzzification.

**Layer 2** is the fuzzification layer. In this layer, the identification block uses a Gaussian membership function in the antecedent part to fuzzify its inputs, while the B-spline membership function is used in the antecedent part of the control block. Therefore, the fuzzy membership function can generally be written as:

$$m_{ij}(x_i) = f(x_i|\chi_1), \tag{9}$$

where $\chi_1$ is the update parameter vector for the antecedent part.

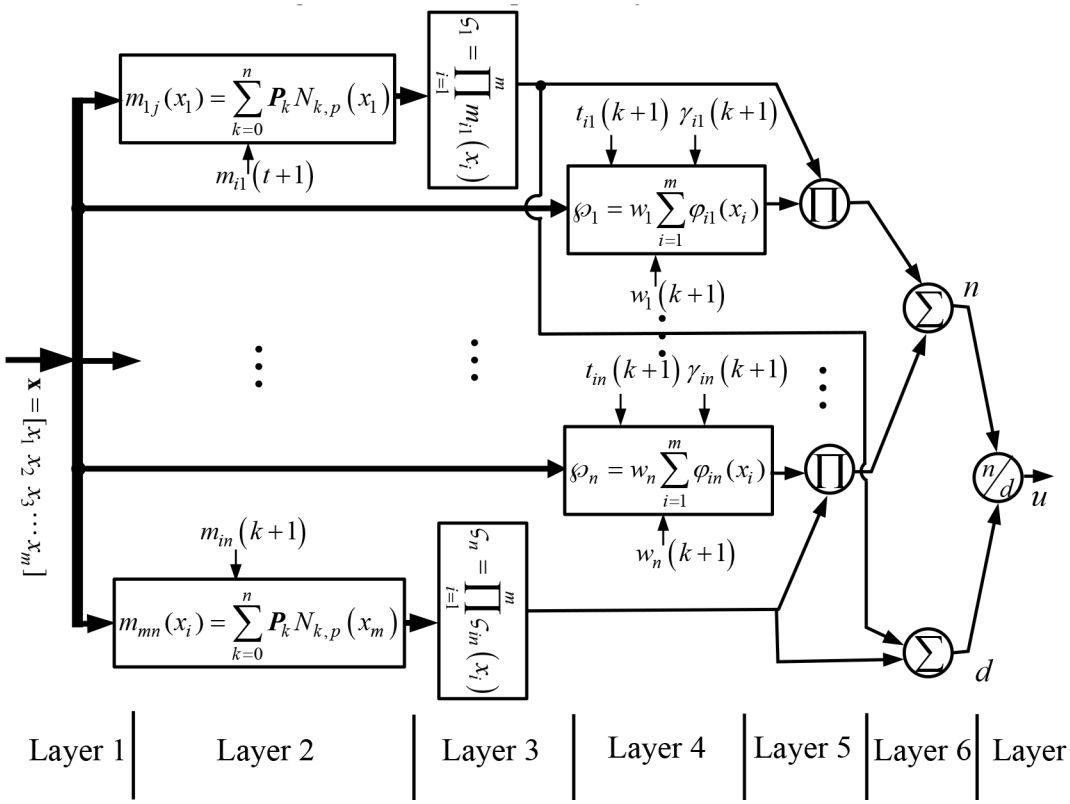


**Figure 3.** ABSWC architecture.

**Layer 3** is the rule layer and calculates the firing strength of each rule by using a T-norm product operator. The output of this layer for $j$th rule is given by:

$$\varsigma_j = \prod_{i=1}^{m} m_{ij}(x_i). \tag{10}$$

**Layer 4** works in parallel with layer 2. Each node of layer 4 is a wavelet network that consists of 3 sublayers: input layer, hidden layer, and output layer. The hidden layer contains the wavelets as activation functions. The output of the wavelet network for the $j$th rule is given by:

$$y_j = \wp_j(x_i|\chi_2) = w_j \sum_{i=1}^{m} \varphi_{ij}(r_{ij}), \tag{11}$$

where $\chi_2$ is the updated parameter vector for the consequent part and $\varphi_{ij}(r_{ij})$ is the Morlet wavelet function given by:

$$\varphi_{ij}(r_{ij}) = \cos(5r_{ij})\, e^{-\frac{r_{ij}^2}{2}}. \tag{12}$$

Here, $r_{ij}(x_i) = \frac{x_i - t_{ij}}{\gamma_{ij}}$, such that $t_{ij}$ and $\gamma_{ij}$ are the translation and dilation factors of $j$th wavelet function.

**Layer 5** is the second layer of the consequent part and multiplies the outputs of the third and fourth layers.

**Layer 6** and **Layer 7** defuzzify the output of layer 5, using the center of gravity method, to calculate the final output of the network. The output of layer 7 is given as:

$$\mathbf{o}=\frac{\sum_{j=1}^{n} \varsigma_j \wp_j}{\sum_{j=1}^{n} \varsigma_j}. \tag{13}$$

Here, $\mathbf{o} \in \{u, y_I\}$ is the output of the network such that $u$ is the output of the control block, and $y_I$ denotes the output of the identification block.

## 4. Parameters update law

The parameters of the identification and control blocks are updated using a backpropagation algorithm based on first-order gradient descent technique. The generalized update law can be defined as follows:

$$\chi_\beta(k+1) = \chi_\beta(k) - \hbar_r^i \frac{\partial \mathbf{J}}{\partial \chi_\beta} + \lambda_r^i \left(\chi_\beta(k) - \chi_\beta(k-1)\right), \tag{14}$$

where $\hbar_r^i$ is the learning rate and $\lambda_r^i$ is the momentum term. The subscript $r$ is used to denote the identification or control block, and the superscript $i$ represents the learning rate and momentum for the respective update parameter. The convergence of the gradient descent algorithm strictly depends upon the value of the learning rate. A low value for the learning rate may lead the algorithm to converge slowly, while a high value results in unstable learning. The momentum term is introduced to smooth the learning process, and its effect on convergence of the algorithm was discussed in detail in [51]. The learning rate and momentum terms are adjusted in the interval ]0 1[. In Eq. (14), $\chi_\beta = [\chi_1\, \chi_2]$ and $\mathbf{J} \in \{J\mathbf{I}, J\mathbf{C}\}$ are the quadratic cost functions, such that $J\mathbf{I}$ and $J\mathbf{C}$ are the cost functions for identification and control blocks, respectively. The subscript $\beta$ is used to denote the identification or control block. The detailed mathematical treatment for update equations of each block is given in the following subsections.

### 4.1. Identification block

The cost function used to update the identification block parameters is given as:

$$J\mathbf{I} = \frac{1}{2}\left[y_I - y\right]^2. \tag{15}$$

$y_I = \frac{\sum_{j=1}^{n} \varsigma_j \wp_j}{\sum_{j=1}^{n} \varsigma_j}$ is the output of the identification block. The identification block uses a Gaussian membership function in the antecedent part and Morlet wavelet function in the consequent part.

The Gaussian membership function is given as:

$$m_{ij}(x_i) = e^{-\left(\frac{x_i - h_{ij}}{\nu_{ij}}\right)^2}, \tag{16}$$

where $h_{ij}$ and $\nu_{ij}$ are the center and width, respectively, for the $j$th membership function of the $i$th input. Therefore, the update parameter vector for the identification block is given as $\chi_I = [h_{ij}\ \nu_{ij}\ w_j\ t_{ij}\ \gamma_{ij}]$. The

generalized parameters' update law can be written as:

$$\chi_I(k+1) = \chi_I(k) - \hbar \frac{\partial J\mathbf{I}}{\partial \chi_I} + \lambda \left(\chi_I(k) - \chi_I(k-1)\right). \tag{17}$$

Here,

$$\frac{\partial J\mathbf{I}}{\partial \chi_I} = \frac{\partial J\mathbf{I}}{\partial y_I}\frac{\partial y_I}{\partial \chi_I} = (y_I - y)\frac{\partial y_I}{\partial \chi_I}. \tag{18}$$

The differential in Eq. (18) can be simplified for the respective parameters using the following chain rule of calculus:

$$\frac{\partial y_I}{\partial h_{ij}} = \frac{\partial y_I}{\partial \varsigma_j}\frac{\partial \varsigma_j}{\partial m_{ij}}\frac{\partial m_{ij}}{\partial h_{ij}}, \tag{19}$$

$$\frac{\partial y_I}{\partial \nu_{ij}} = \frac{\partial y_I}{\partial \varsigma_j}\frac{\partial \varsigma_j}{\partial m_{ij}}\frac{\partial m_{ij}}{\partial \nu_{ij}}, \tag{20}$$

$$\frac{\partial y_I}{\partial t_{ij}} = \frac{\partial y_I}{\partial \wp_j}\frac{\partial \wp_j}{\partial \varphi_{ij}}\frac{\partial \varphi_{ij}}{\partial r_{ij}}\frac{\partial r_{ij}}{\partial t_{ij}}, \tag{21}$$

$$\frac{\partial y_I}{\partial \gamma_{ij}} = \frac{\partial y_I}{\partial \wp_j}\frac{\partial \wp_j}{\partial \varphi_{ij}}\frac{\partial \varphi_{ij}}{\partial r_{ij}}\frac{\partial r_{ij}}{\partial \gamma_{ij}}, \tag{22}$$

$$\frac{\partial y_I}{\partial w_{ij}} = \frac{\partial y_I}{\partial \wp_j}\frac{\partial \wp_j}{\partial w_{ij}}. \tag{23}$$

After simplifying these differentials, the final updated equations for each parameter of the identification block can be written as follows:

$$h_{ij}(k+1) = h_{ij}(k) - \hbar (y_I - y)\, 2\frac{\varsigma_j(x_i)}{\sum_{j=1}^{n}\varsigma_j(x_i)}(\wp_j - y_I)\frac{x_i - h_{ij}}{\nu_{ij}^2} + \lambda\left(h_{ij}(k) - h_{ij}(k-1)\right), \tag{24}$$

$$\nu_{ij}(k+1) = \nu_{ij}(k) - \hbar (y_I - y)\, 2\frac{\varsigma_j(x_i)}{\sum_{j=1}^{n}\varsigma_j(x_i)}(\wp_j - y_I)\frac{(x_i - h_{ij})^2}{\nu_{ij}^3} + \lambda\left(\nu_{ij}(k) - \nu_{ij}(k-1)\right), \tag{25}$$

$$t_{ij}(k+1) = t_{ij}(k) - \hbar (y_I - y)\frac{\varsigma_j(x_i)}{\sum_{j=1}^{n}\varsigma_j(x_i)}\frac{\left(r_{ij}\wp_{ij} + 5w_j \sin(5r_{ij})\, e^{-\frac{r_{ij}^2}{2}}\right)}{\gamma_{ij}} + \lambda\left(t_{ij}(k) - t_{ij}(k-1)\right), \tag{26}$$

$$\gamma_{ij}(k+1) = \gamma_{ij}(k) - \hbar (y_I - y)\frac{\varsigma_j(x_i)}{\sum_{j=1}^{n}\varsigma_j(x_i)}\frac{r_{ij}\left(r_{ij}\wp_{ij} + 5w_j \sin(5r_{ij})\, e^{-\frac{r_{ij}^2}{2}}\right)}{\gamma_{ij}} + \lambda\left(\gamma_{ij}(k) - \gamma_{ij}(k-1)\right), \tag{27}$$

$$w_{ij}(k+1) = w_{ij}(k) - \hbar (y_I - y)\frac{\varsigma_j(x_i)}{\sum_{j=1}^{n}\varsigma_j(x_i)}\wp_{ij}(x_i) + \lambda\left(w_{ij}(k) - w_{ij}(k-1)\right). \tag{28}$$

### 4.2. Control block

The control block utilizes B-spline membership functions in the antecedent part and Morlet wavelet functions in the consequent part, as given in Eq. (12). The B-spline membership function is formed by the weighted sum of the blending functions and is given as:

$$m_{ij}(x_i) = \sum_{k=0}^{n} \mathbf{P}_k N_{k,p}(x_i) \qquad 1 \le p \le n. \tag{29}$$

Here, $m_{ij}$ is the degree of membership function, and $\boldsymbol{P}_k$ is the control point with $k = 0, 1, 2, 3 \cdots, n$ such that the total number of control points is $n + 1$. $p$ is the order of the B-spline basis function. $N_{k,p}(x_i) = N(x_i|\tau_1, \tau_2, \cdots, \tau_{n+p})$ is the $k$th B-spline basis function and is given by the following Cox–de Boor recursion formula:

$$N_{k,p}(x) = \begin{cases} 1 \text{ if } p = 1, \quad x \in [\tau_i \ \tau_{i+1}[ \\ \left(\frac{x-\tau_i}{\tau_{i+p-1}-\tau_i}\right) N_{i,p-1} + \left(\frac{\tau_{i+p}-x}{\tau_{i+p}-\tau_{i+1}}\right) N_{i+1,p-1} \text{ if } p > 1, \quad x \in [\tau_i \ \tau_{i+p}[ \\ 0 \text{ if } p = 1, \quad x \notin [\tau_i \ \tau_{i+1}[ \end{cases} . \tag{30}$$

$\tau = [\tau_1 \ \tau_2 \cdots \tau_{k+p}] \in \mathrm{R}$ is the knot vector such that $\tau_{i+1} - \tau_i \ge 0$. For any input $x \in [a \ b] \to \mathrm{R}$, the knot sequence is defined as $\left\{ \underbrace{a, a, \cdots, a}_{p-terms}, \tau_p, \cdots, \tau_n, \underbrace{b, b, \cdots, b}_{p-terms} \right\}$. The number of control points and types of knots are of primary importance for the smoothness of the B-spline membership function.

In this work, the B-spline membership function of order 2 that corresponds to the locally controllable triangular membership function has been used with 9 control points and 13 knot vectors. The control points are evenly distributed over the membership function with fixed knot sequence.

The parameters of the control block are updated by minimizing the following cost function:

$$J\mathbf{C} = \frac{1}{2}\left[(y_r - y)^2 + \lambda u^2\right], \tag{31}$$

where $u$ is the control effort and $\lambda$ is the weighting factor introduced for optimal adjustment of the controller output. Eq. (14), for the control block, can be written as follows:

$$\chi_C(k+1) = \chi_C(k) - \hbar \frac{\partial J\mathbf{C}}{\partial \chi_C} + \lambda \left(\chi_C(k) - \chi_C(k-1)\right). \tag{32}$$

The term $\frac{\partial J\mathbf{C}}{\partial \chi_C}$ in Eq. (32) can be simplified using the following relation:

$$\frac{\partial J\mathbf{C}}{\partial \chi_C} = -\left[(y_r - y)\frac{\partial y}{\partial u} - \lambda u\right]\frac{\partial u}{\partial \chi_C}, \tag{33}$$

where $\chi_C = [m_{ij} \ w_j \ t_{ij} \ \gamma_{ij}]$ is the adaptation parameter vector for the control block. The output of the control block is $u = \frac{\sum_{j=1}^{n} \varsigma_j \wp_j}{\sum_{j=1}^{n} \varsigma_j}$. The differential in Eq. (33) can be simplified, for respective parameters, using the following

chain rule of calculus:

$$\frac{\partial u}{\partial m_{ij}} = \frac{\partial u}{\partial \varsigma_j}\frac{\partial \varsigma_j}{\partial m_{ij}}, \tag{34}$$

$$\frac{\partial u}{\partial t_{ij}} = \frac{\partial u}{\partial \wp_j}\frac{\partial \wp_j}{\partial \varphi_{ij}}\frac{\partial \varphi_{ij}}{\partial r_{ij}}\frac{\partial r_{ij}}{\partial t_{ij}}, \tag{35}$$

$$\frac{\partial u}{\partial \gamma_{ij}} = \frac{\partial u}{\partial \wp_j}\frac{\partial \wp_j}{\partial \varphi_{ij}}\frac{\partial \varphi_{ij}}{\partial r_{ij}}\frac{\partial r_{ij}}{\partial \gamma_{ij}}, \tag{36}$$

$$\frac{\partial u}{\partial w_{ij}} = \frac{\partial u}{\partial \wp_j}\frac{\partial \wp_j}{\partial w_{ij}}. \tag{37}$$

Eqs. (35), (36), and (37) are the same as those of the identification block due to similar network architecture, the only difference is Eq. (34) for B-spline membership function that can be simplified as:

$$\frac{\partial u}{\partial m_{ij}} = \frac{\varsigma_j(x_i)}{m_{ij}\sum_{j=1}^{n}\varsigma_j(x_i)}(\wp_j - u). \tag{38}$$

The final update equations for each parameter of the control block can be written as follows:

$$m_{ij}(k+1) = m_{ij}(k) + \hbar\left[(y_r - y)\frac{\partial y}{\partial u} - \lambda u\right]\frac{\varsigma_j(x_i)}{m_{ij}\sum_{j=1}^{n}\varsigma_j(x_i)}(\wp_j - u) + \lambda\left(m_{ij}(k) - m_{ij}(k-1)\right), \tag{39}$$

$$t_{ij}(k+1) = t_{ij}(k) + \hbar\left[(y_r - y)\frac{\partial y}{\partial u} - \lambda u\right]\frac{\varsigma_j(x_i)}{\sum_{j=1}^{n}\varsigma_j(x_i)}\frac{\left(r_{ij}\wp_{ij} + 5w_j\sin(5r_{ij})\,e^{-\frac{r_{ij}^2}{2}}\right)}{\gamma_{ij}} + \lambda\left(t_{ij}(k) - t_{ij}(k-1)\right), \tag{40}$$

$$\gamma_{ij}(k+1) = \gamma_{ij}(k) + \hbar\left[(y_r - y)\frac{\partial y}{\partial u} - \lambda u\right]\frac{\varsigma_j(x_i)}{\sum_{j=1}^{n}\varsigma_j(x_i)}\frac{r_{ij}\left(r_{ij}\wp_{ij} + 5w_j\sin(5r_{ij})\,e^{-\frac{r_{ij}^2}{2}}\right)}{\gamma_{ij}} + \lambda\left(\gamma_{ij}(k) - \gamma_{ij}(k-1)\right), \tag{41}$$

$$w_{ij}(k+1) = w_{ij}(k) + \hbar\left[(y_r - y)\frac{\partial y}{\partial u} - \lambda u\right]\frac{\varsigma_j(x_i)}{\sum_{j=1}^{n}\varsigma_j(x_i)}\wp_j(x_i) + \lambda\left(w_{ij}(k) - w_{ij}(k-1)\right). \tag{42}$$

The plant output sensitivity measure $\frac{\partial y}{\partial u}$ in the above equations is provided by the identification block and is given as:

$$\frac{\partial y}{\partial u} = \frac{\sum_{j=1}^{n}\varsigma_j\left[\frac{-2(u-h_{1j})(\wp_j - y)}{\sigma_{1j}^2} - \frac{5w_j\sin 5r_{1j}e^{-\frac{r_{ij}^2}{2}}}{\gamma_{1j}} - \frac{w_j r_{1j}\varphi_{1j}}{\gamma_{1j}}\right]}{\sum_{j=1}^{n}\varsigma_j}. \tag{43}$$

## 5. Online adaptive algorithm

The parameters of the control and identification block are updated using the following online adaptive algorithm.

**Step 1:** The parameters of the control and identification block are initialized and a reference value is assigned.

**Step 2:** The values of learning rates and momentum terms are adjusted.

**Step 3:** The inputs to the control block are sampled at the $k$th time instant.

**Step 4:** The parameters of identification block are updated by minimizing $J\!I(k)$ using $y$ and $y_I$.

**Step 5:** The output of the controller is calculated and applied to the plant.

**Step 6:** The output of the plant is predicted by the identification block at the $(k+1)$th instant using $u(k)$.

**Step 7:** Based on $y_I$, the adaptation error is calculated and backpropagated through the control block to update its parameters by minimizing $J\!C$.

**Step 8:** If the solution converges, repeat steps 3–7 until the required tolerance value is achieved; otherwise, repeat steps 2–7.

The adaptation errors for both the identification and control blocks are scalar values and are calculated once during a single iteration, which makes the controller computationally efficient. The proposed control scheme has been analyzed both with and without incorporation of the identification block. For ABSWC, the term $\frac{\partial y}{\partial u}$ is taken as 1 [52].

## 6. Stability analysis of the proposed control strategy

The stability of the proposed control system is discussed in this section for the identification and control blocks, since the convergence of gradient descent depends upon the choice of learning rate. This section presents the range for defining the learning rates for respective update parameters based on Lyapunov function.

### 6.1. Stability analysis for identification block

Define a Lyapunov function given as:

$$V_I = \frac{1}{2}\left[E\mathbf{I}\right]^2, \tag{44}$$

where $E\mathbf{I}$ is the adaptation error for the identification block given as:

$$E\mathbf{I} = (y - y_I). \tag{45}$$

The change in Lyapunov function is given as in [53]:

$$\Delta V_I = V_I(k+1) - V_I(k) = \frac{1}{2}\left[E\mathbf{I}^2(k+1) - E\mathbf{I}^2(k)\right]. \tag{46}$$

The change in learning error is given as:

$$\Delta E\mathbf{I}(k) = E\mathbf{I}(k+1) - E\mathbf{I}(k) \approx \left(\frac{\partial E\mathbf{I}(k)}{\partial \chi_I}\right)^T \Delta\chi_I \tag{47}$$

$$= \begin{pmatrix} \frac{\partial E\mathbf{I}}{\partial h_I} & \frac{\partial E\mathbf{I}}{\partial \nu_I} & \frac{\partial E\mathbf{I}}{\partial t_I} & \frac{\partial E\mathbf{I}}{\partial \gamma_I} \frac{\partial E\mathbf{I}}{\partial w_I} \end{pmatrix} \begin{pmatrix} \Delta h_I \\ \Delta \nu_I \\ \Delta t_I \\ \Delta \gamma_I \\ \Delta w_I \end{pmatrix}, \tag{48}$$

using $\Delta\chi_{I_i} = -\hbar_I^{i_i} \frac{\partial J\mathbf{I}}{\partial \chi_{I_i}} = \hbar_I^{i_i} E\mathbf{I}(k) \frac{\partial y_I}{\partial \chi_{I_i}}$

$$\Rightarrow \begin{pmatrix} \Delta h_I \\ \Delta \nu_I \\ \Delta t_I \\ \Delta \gamma_I \\ \Delta w_I \end{pmatrix} = E\mathbf{I}(k) \begin{pmatrix} \hbar_I^h \frac{\partial y_I}{\partial h_I} \\ \hbar_I^\nu \frac{\partial y_I}{\partial \nu_I} \\ \hbar_I^t \frac{\partial y_I}{\partial t_I} \\ \hbar_I^\gamma \frac{\partial y_I}{\partial \gamma_I} \\ \hbar_I^w \frac{\partial y_I}{\partial w_I} \end{pmatrix}. \tag{49}$$

The convergence theorem for identification block can then be defined as follows:

**Theorem 1** *The asymptotic convergence is guaranteed if $\hbar_I^{i_i}$ is chosen to satisfy the following condition:*

$$0 < \hbar_I^{i_i} < \frac{2}{\max \left( \frac{\partial y_I}{\partial \chi_I^i} \right)^2}. \tag{50}$$

*The proof of this theorem is given in the Appendix.*

### 6.2. Stability analysis for control block

Define a Lyapunov function for control block as:

$$V_C = \frac{1}{2} \left[ E\mathbf{C} \right]^2, \tag{51}$$

where $E\mathbf{C}$ is the adaptation error for the control block, given as:

$$E\mathbf{C} = \left[ (y_r - y) \frac{\partial y}{\partial u} - \lambda u \right]. \tag{52}$$

The change in Lyapunov function is given as:

$$\Delta V_C = V_C(k+1) - V_C(k) = \frac{1}{2} \left[ E\mathbf{C}^2(k+1) - E\mathbf{C}^2(k) \right]. \tag{53}$$

The change in learning error is given as:

$$\Delta E\mathbf{C}(k) = E\mathbf{C}(k+1) - E\mathbf{C}(k) \approx \left( \frac{\partial E\mathbf{C}(k)}{\partial \chi_C} \right)^T \Delta\chi_C, \tag{54}$$

$$= \begin{pmatrix} \frac{\partial E\mathbf{C}}{\partial m_C} & \frac{\partial E\mathbf{C}}{\partial \nu_C} & \frac{\partial E\mathbf{C}}{\partial t_C} & \frac{\partial E\mathbf{C}}{\partial \gamma_C} \end{pmatrix} \begin{pmatrix} \Delta m_C \\ \Delta \nu_C \\ \Delta t_C \\ \Delta \gamma_I \end{pmatrix}, \tag{55}$$

using $\Delta\chi_{C_i} = -\hbar_C^{i_i} \frac{\partial J\mathbf{C}}{\partial \chi_{C_i}} = \hbar_C^{i_i} E\mathbf{C}(k) \frac{\partial u}{\partial \chi_{C_i}}$

$$\Rightarrow \begin{pmatrix} \Delta m_C \\ \Delta t_C \\ \Delta \gamma_C \\ \Delta w_C \end{pmatrix} = E\mathbf{C}(k) \begin{pmatrix} \hbar_C^m \frac{\partial u}{\partial m_C} \\ \hbar_C^t \frac{\partial u}{\partial t_C} \\ \hbar_C^\gamma \frac{\partial u}{\partial \gamma_C} \\ \hbar_C^w \frac{\partial u}{\partial w_C} \end{pmatrix}. \tag{56}$$

The convergence theorem for the control block can then be defined as follows.

**Theorem 2** *The asymptotic convergence is guaranteed if $\hbar_C^{i_i}$ is chosen to satisfy the following condition:*

$$0 < \hbar_C^i < \frac{2}{\left[\left(\frac{\partial y}{\partial u}\right)^2 + \lambda\right] \left(\max\left(\frac{\partial u}{\partial \chi_C^i}\right)\right)^2}. \tag{57}$$

*The proof of this theorem is given in the Appendix.*

**Remark** Since the sensitivity term in Eq. (57) is provided by the identifier, to meet the convergent conditions of Theorem 1 and Theorem 2, term $\frac{\partial y}{\partial u}$ is replaced by $\mathrm{S}_{\max}$ [53], such that:

$$\begin{aligned}
\mathrm{S}_{\max} &= \max\left(\frac{\partial y}{\partial u}\right) \\
&= \max\left( \frac{\sum_{j=1}^{n} \varsigma_j \left[ \frac{-2(u-h_{1j})(\wp_j - y)}{\sigma_{1j}^2} - \frac{5w_j \sin 5r_{1j} e^{-\frac{r_{ij}^2}{2}}}{\gamma_{1j}} - \frac{w_j r_{1j} \varphi_{1j}}{\gamma_{1j}} \right]}{\sum_{j=1}^{n} \varsigma_j} \right) \\
&\leq \max\left| \frac{-2(u-h_{1j})(\wp_j - y)}{\sigma_{1j}^2} - \frac{5w_j \sin 5r_{1j} e^{-\frac{r_{ij}^2}{2}}}{\gamma_{1j}} - \frac{w_j r_{1j} \varphi_{1j}}{\gamma_{1j}} \right| \\
&\leq \max\left| \frac{2(M-h_{1j})(\wp_j - y)}{\sigma_{1j}^2} + \frac{6w_{j\max}}{\gamma_{1j\min}} \right| \\
&\leq \left| \frac{2(M-h_{1j\min})(\wp_{j\max} - y)}{\sigma_{1j\min}^2} + \frac{6w_{j\max}}{\gamma_{1j\min}} \right|,
\end{aligned}$$

where $M$ is the upper bound on control effort, i.e. 0.2 p.u.; $m$ is the number of inputs; and $n$ is the number of rules.

## 7. Results and discussion

The robustness of the proposed control system has been checked using a multimachine test system with SSSC installed in the middle of the system. The system consists of 2 areas with 2 generating units in each area, as shown in Figure 2 as "plant". Generators 1 and 2 are in area 1, while generators 3 and 4 are in area 2. The generators in the power system are equipped with a hydraulic turbine governor (HTG) and excitation system. The HTG is a nonlinear hydraulic turbine model, and the governor system is based on the PID and servomotor. A voltage regulator and DC exciter form the excitation system. PSSs installed on each machine are disabled. Details of system parameters and machines ratings are given in [54]. MATLAB/Simulink is used as a simulation tool to generate the results. The phasor simulation method is used for transient stability analysis of the system. The phasor simulation method improves the simulation speed by replacing the differential equations with simple algebraic equations, ignoring the fast electromechanical transients, and is hence suitable for simulating large power systems. Continuous variable-step solver ode23tb with a maximum time step of 1 cycle of fundamental frequency (i.e. 60 Hz) is used with this simulation method.

The simulations were carried out for 4 cases: SSSC installed in the system with no supplementary damping control, SSSC installed with conventional adaptive TSK control with no identification block (ATSC), SSSC installed with ABSWC, and SSSC installed with ABSWC with identification (ABSWCI). The membership functions for each input and number of rules for control and identification block is 2. Therefore, the total numbers of parameters to be updated for ABSWCI and ABSWC are 32 and 14, respectively. The relative rotor speed deviation and its derivative are taken as 2 inputs to the control block, while the output of the controller is the series injected voltage. The controller output and delayed output of the plant are inputs to the identification block.

In order to check the robustness of the proposed control system for small and large disturbances, variation in fault location and duration, structural changes, and the online stability of the system, a series of faults is applied to the system. A 3-phase, self-clearing fault of 8 cycles in duration is applied at t = 1 s on 1 of the 3 tie lines near area 2. Another 3-phase fault of the same duration is applied in area 2 near bus $B_8$ at t = 12 s, followed by a 3-phase, self-clearing fault of 12 cycles in duration on 1 of the tie lines at t = 21 s. The last fault is a double line outage near area 1, at t = 28 s. The results for local and interarea modes of oscillations are shown in Figures 4a–4d, respectively. The application of the first 3-phase fault makes the system unstable in the case of no control and causes the simulation to stop at t = 9.5 s. A comparison of the results shows that ABSWCI has better performance for large disturbances as compared to small disturbances and is therefore more suitable for systems with higher nonlinearities.

Figures 5a and 5b show the power flow on 1 of the 3 tie lines measured at buses $B_4$ and $B_6$, respectively. Initially, there is a power flow of almost 413 MW from area 1 to area 2. ATSC has poorly damped oscillatory behavior for postfault power damping, whereas ABSWCI has significantly better results as compared to ABSWC and ATSC. The control effort, shown in Figure 5c, reveals that in the case of ABSWCI, the injected voltage does not hit the maximum allowable limit, thus reducing the megaVAR ratings of the converter and making the system cost-effective. Plant output sensitivity measurement is shown in Figure 5d, depicting the dynamic behavior of the plant at the time of the fault.

Although there is performance improvement for ABSWCI, it can be seen that ABSWC, being already an intelligent, nonlinear, and adaptive control, has competent results, and performance improvement for ABSWCI is difficult to analyze in nonlinear time-domain simulations, especially for local modes of oscillations. Therefore, the performance has been quantified in terms of different performance indices to get clear insight into the results in the transient and steady-state regions. The performance index can be defined as the integral of a function of

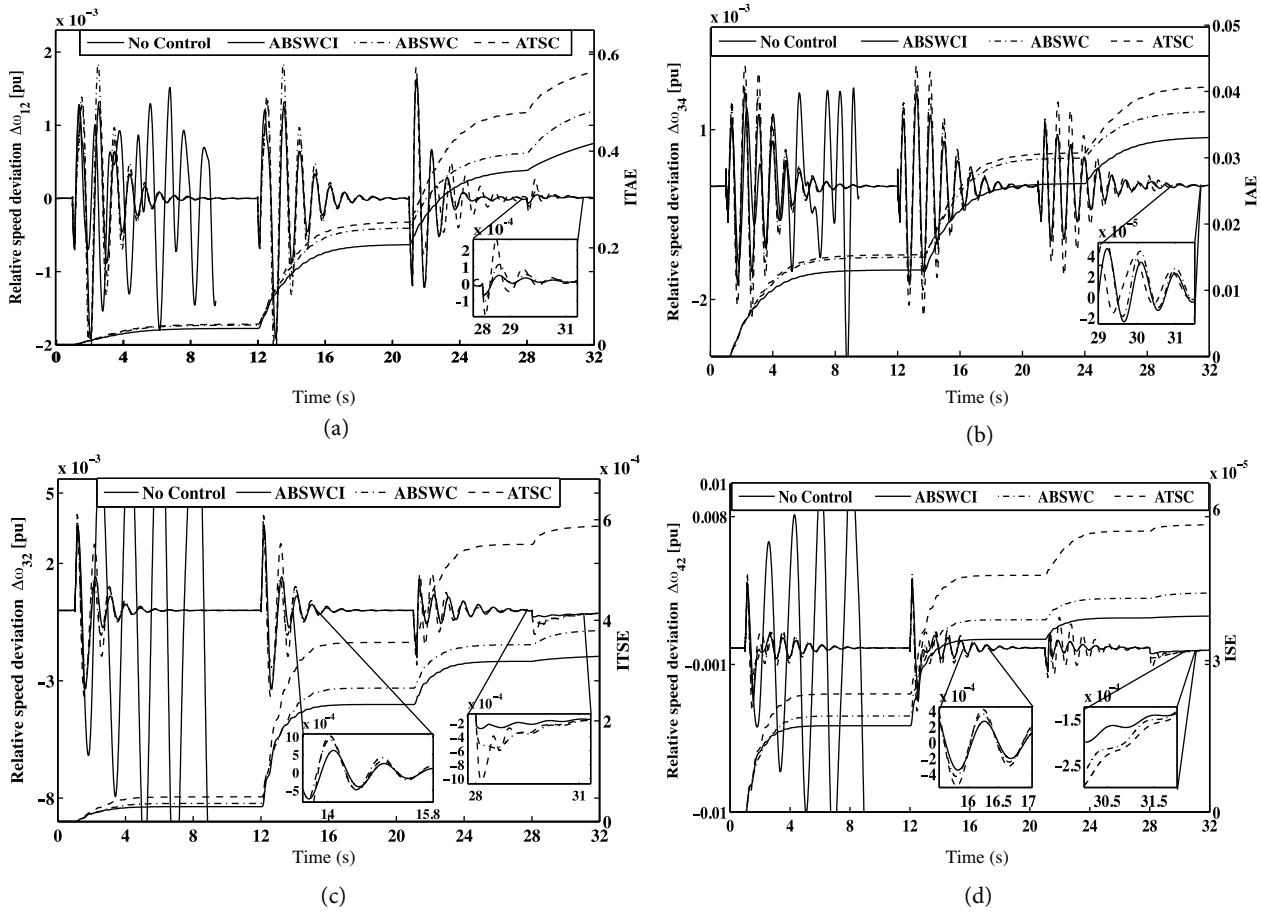


**Figure 4.** Multimachine test system: (a) and (b) local modes of oscillations; (c) and (d) interarea modes of oscillations.

time, and error is given as:

$$PI_{j,k} = \int_0^{t_s} t^j \left( \sum_{i=1}^{n} \left( |\Delta\omega_{L_i}|^k + |\Delta\omega_{I_i}|^k \right) \right) dt. \tag{58}$$

Here, $t_s$ is the total simulation time and $i$ is the mode number. $L$ and $I$ represent the local and interarea modes of oscillations, respectively. $k$ and $j$ are fixed numbers, such that $(k, j) \in \{(1,1), (1,0), (2,1), (2,0)\}$ for integral time absolute error (ITAE), integral absolute error (IAE), integral time square error (ITSE), and integral square error (ISE), respectively.

These performance indices are shown in Figures 4a–4d, with the y-axis on the right. These performance indices give a clear picture of performance improvement for ABSWCI as compared to ABSWC, showing that ABSWCI has improved performance results in transient and steady-state regions for both local and interarea modes of oscillations. The quantitative results for these performance indices are given in the Table. The statistics show that the performance improvement for ITSE and ISE is greater than for ITAE and IAE, highlighting the more pronounced effect of ABSWCI in the transient region.

Another performance measure used to investigate the performance of the proposed control system is the smoothness of the control effort. The smoothness of the control effort reduces the switching losses of the converter. Figure 5c shows the nonlinear time domain simulation results for control effort as injected voltage

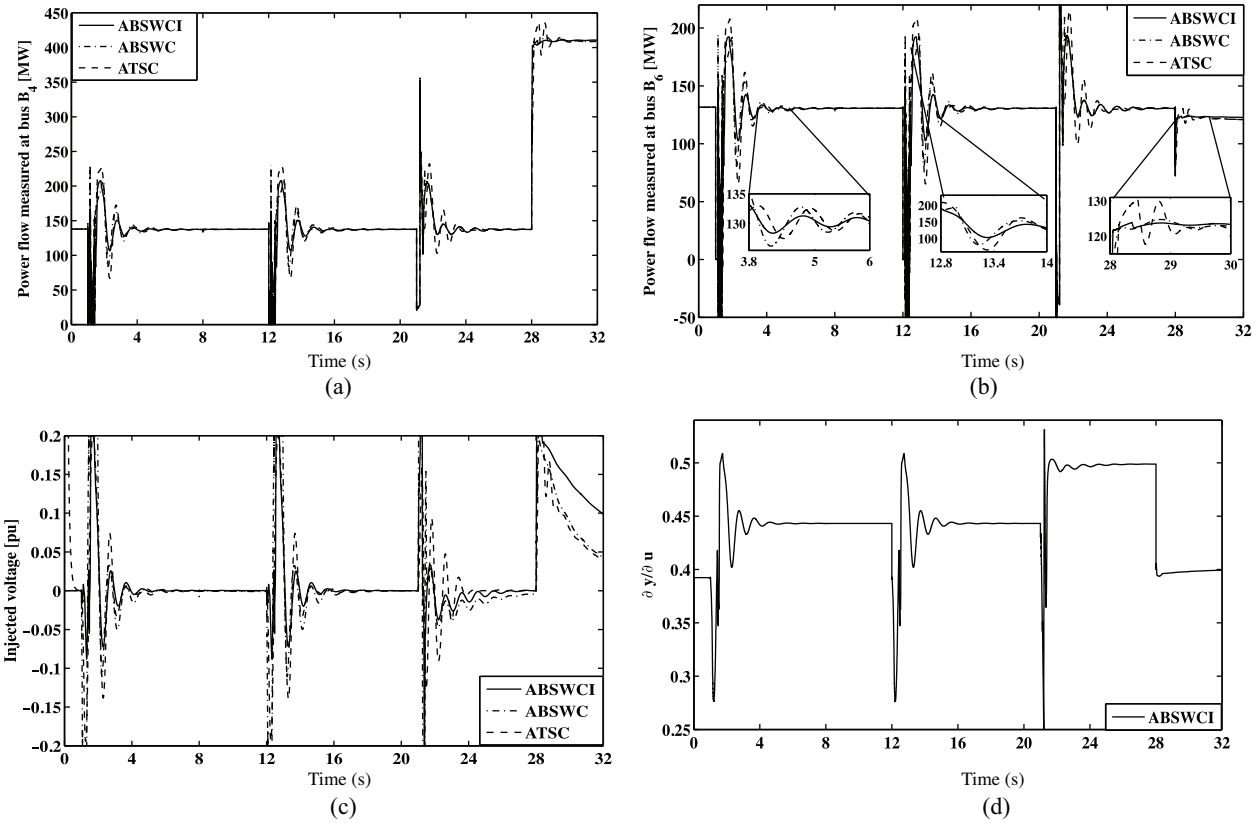


**Figure 5.** Multimachine test system: (a) line power flow measured at bus $B_4$; (b) line power flow measured at bus $B_6$; (c) control effort; (d) sensitivity measure.

**Table.** Comparative results with respect to ATSC.

| Control Algorithm | Performance improvement [%] | | | | Control effort smoothness | | |
|---|---|---|---|---|---|---|---|
| | ITAE | ITSE | IAE | ISE | ABSWCI | ABSWC | ATSC |
| ABSWCI | 30.71 | 42.20 | 26.85 | 36.18 | 477.02 | 1035 | 1581 |
| ABSWC | 23.83 | 36.21 | 18.19 | 29.76 | | | |

for ABSWC and ABSWCI. The smoothness measure is calculated as follows:

$$S_M = \sqrt{\frac{1}{L}\sum_{i=1}^{L}\left[\Lambda^2 u\left(i\right)\right]^2} \tag{59}$$

where, $L$ is the total length of the control signal and $\Lambda^2$ is the discrete second-order derivative. The smaller the value of this smoothness measure is, the smoother the control effort will be [55], which is given quantitatively in the Table. Figure 5d shows the plant sensitivity measure using ABSWCI; in the case of ABSWC, this term is taken as constant. In other words, ABSWC shows a static picture of the system to the controller, while ABSWCI updates the control block parameters based on the online sensitivity measure of the system, clearly depicting the dynamics of the system and hence improving the damping performance with smooth control effort.

To get a clear idea of frequency behaviors, the results for local and interarea modes of oscillations and

control effort for case 2 were analyzed in time-frequency domain for both ABSWC and ABSWCI. For this purpose, SPWVD has been used. SPWVD reduces the effect of interference terms present in WVD and is given as:

$$SPWVD_x(k,\omega) = \int_{-\infty}^{\infty} h(\tau) \int g(u-k)\, x(u+\tau/2)\, x*(u-\tau/2)\, du e^{-j\omega\tau} d\tau \tag{60}$$

Here, $h(\tau)$ is the frequency smoothing window in the time domain used to reduce the effect of cross-terms, and eliminates the integration over $]-\infty\ \infty]$ for WVD. $g(k)$ is the smoothing function for the time domain [56].

The results for this analysis are presented in Figure 6. The figures in the first column show the results for ABSWC; the results for ABSWCI are shown in the second column. It is interesting to see that SPWVD more clearly shows the frequency domain behavior of signals in time. Figures 6a–6d show that both control techniques have almost the same spectra for local modes of oscillations; however, the magnitude of low frequencies ranging from 0.05 to 0.15 Hz is smaller in the case of ABSWCI as compared to ABSWC. Figures 6e–6h show that ABSWCI successfully damps some relatively high frequencies in the range of 0.2 to 0.25 Hz; for ABSWC, these frequencies are present with small amplitude. Moreover, Figures 6g and 6h show that the low frequencies in the range of 0.1 to 0.15 Hz have high amplitude in the case of ABSWC as compared to ABSWCI. In addition, very low frequencies, below 0.05 Hz, are observable for the fourth fault between 25 to 28 s in the case of ABSWC.

Most importantly, the spectra of control efforts for both control algorithms shown in Figures 6i and 6j reveal that the control effort for ABSWC has high frequencies in the range of 0.1 to 0.25 Hz with observable amplitude as compared to that of ABSWCI. ABSWCI has very small value, almost negligible, for high frequencies, and some low frequencies below 0.05 Hz are present for the last fault, with significant amplitude showing that the transitions in the control signal are smooth.

## 8. Conclusion

This paper presents the application and comparison of an optimal direct and indirect adaptive neuro-fuzzy control scheme to damp power system oscillations using the SSSC. Low-frequency oscillations, being a constant threat to the secure and reliable operation of power systems, were studied and discussed. A detailed literature survey along with solution methods for damping low frequency oscillations using SSSC was presented. A hybrid adaptive neuro-fuzzy B-spline wavelet-based control technique was proposed and successfully applied to a multimachine power system for damping local and interarea modes of oscillations. Detailed mathematical modeling for the power system installed with the SSSC and the proposed control scheme was given. The performance of the proposed control scheme was optimized in terms of smoothness of the control effort by introducing the identification block. It is to be noted that adaptation errors for identification and control blocks are scalars, which makes the proposed scheme computationally efficient and highly suitable for real-time implementation.

Moreover, the proposed control scheme eliminates the need for installation of a PSS on each machine, which eventually makes the system cost-efficient compared to those installed with both. This also improves the simplicity of the control scheme, as the interaction between the PSS and SSSC need not be considered. The MATLAB/Simulink simulation environment was used to generate the results for different fault scenarios. The results were analyzed on the basis of nonlinear time-domain simulations, performance indices, and time-frequency domain representation using SPWVD. It was found that inclusion of the identification block in the proposed control scheme improves the smoothness of the control effort, preserving the damping performance in transient and steady-state regions for all of the discussed scenarios. The SPWVD analysis shows the smaller

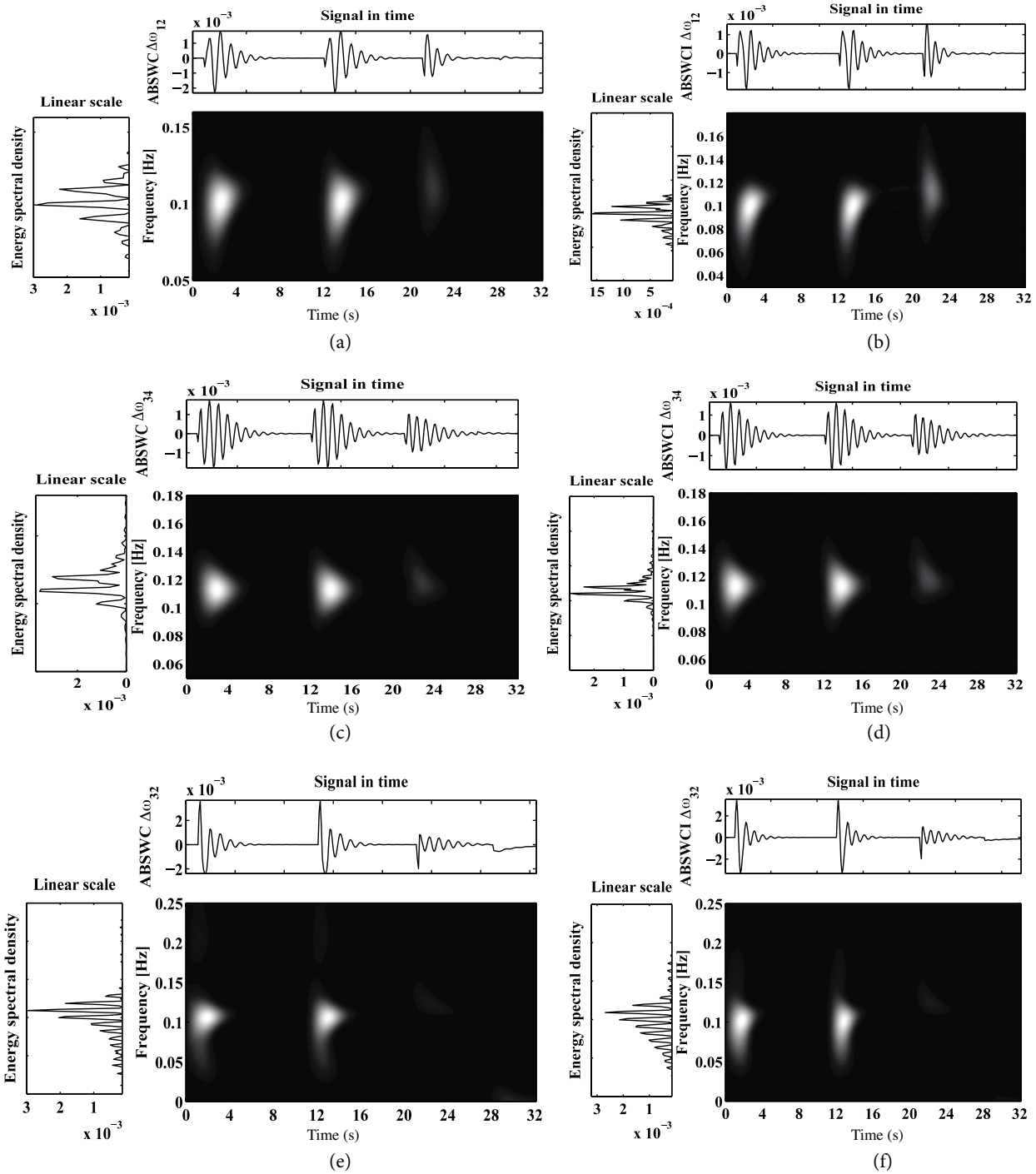


**Figure 6.** SPWVD analysis: (a), (c), (e), and (g) local and interarea modes of oscillations with ABSWC; (b), (d) and (f), and (h) local and interarea modes of oscillations with ABSWCI; (i) control effort for ABSWC; (j) control effort for ABSWCI.

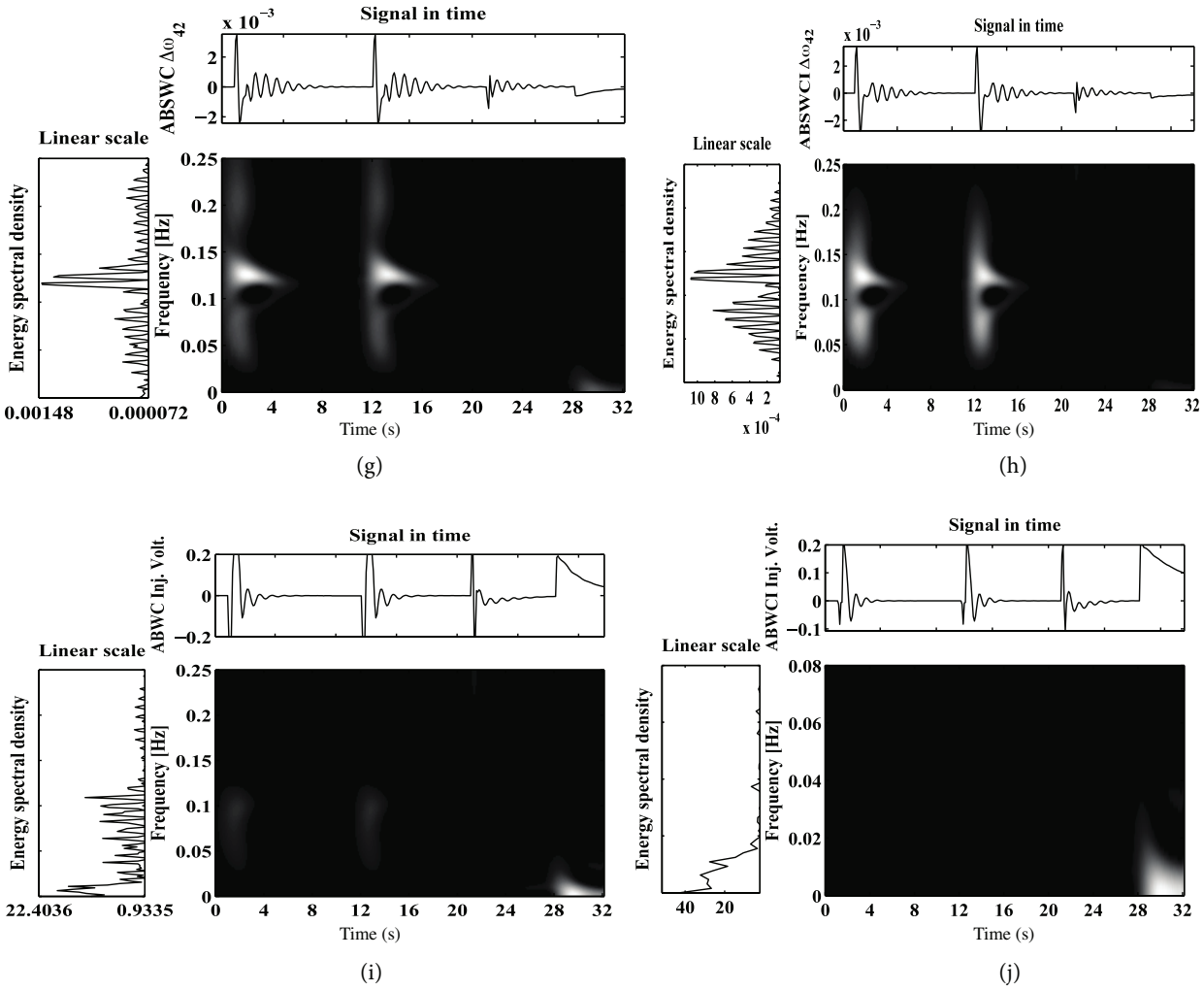


**Figure 6.** Continued.

amplitude of high frequencies in the control effort signal in the case of ABSWCI. The smoothness of the control effort reduces the switching losses and megaVAR ratings of the converter. Since the proposed control scheme is not application-specific, its application horizon can further be extended to other nonlinear, time-varying plants.

## 9. Future work

A number of neuro-fuzzy wavelet-based adaptive control techniques have been proposed in the literature for nonlinear, dynamic plants. A comparison of ABSWCI with some of them on the basis of control effort smoothness and complexity of the control scheme would be an interesting future dimension.

The proposed control scheme uses a gradient-descent–based backpropagation algorithm for parameter adaptation; some other sophisticated techniques can also be investigated for performance improvement. The performance analysis of the proposed control scheme for large power systems would also be a logical extension of this work.

## Appendix

### Proof of Theorem 1

According to Eq. (46), the change in Lyapunov function is given as:

$$\Delta V_I = V_I(k+1) - V_I(k) = \frac{1}{2}\left[E\mathbf{I}^2(k+1) - E\mathbf{I}^2(k)\right]. \tag{A1}$$

Using Eq. (47),

$$\Delta V_I = \Delta E\mathbf{I}(k)\left[E\mathbf{I}(k) + \frac{1}{2}\Delta E\mathbf{I}(k)\right]. \tag{A2}$$

Using Eq. (47) and $\Delta\chi_{I_i} = -\hbar_I^{i_i}\frac{\partial J\mathbf{I}}{\partial\chi_{I_i}} = \hbar_I^{i_i}E\mathbf{I}(k)\frac{\partial y_I}{\partial\chi_{I_i}}$ in Eq. (A2),

$$\Delta V_I = \left(\frac{\partial E\mathbf{I}(k)}{\partial\chi_I}\right)^T \hbar_I E\mathbf{I}(k)\frac{\partial y_I}{\partial\chi_I}\left\{E\mathbf{I}(k) + \frac{1}{2}\left(\frac{\partial E\mathbf{I}(k)}{\partial\chi_I}\right)^T \hbar_I E\mathbf{I}(k)\frac{\partial y_I}{\partial\chi_I}\right\}. \tag{A3}$$

Using Eq. (46),

$$\frac{\partial E\mathbf{I}}{\partial\chi_I} = -\frac{\partial y_I}{\partial\chi_I} \tag{A4}$$

$$\Rightarrow \Delta V_I = -\left(\frac{\partial y_I}{\partial\chi_I}\right)^T \hbar_I E\mathbf{I}(k)\frac{\partial y_I}{\partial\chi_I}\left\{E\mathbf{I}(k) - \frac{1}{2}\left(\frac{\partial y_I}{\partial\chi_I}\right)^T \hbar_I E\mathbf{I}(k)\frac{\partial y_I}{\partial\chi_I}\right\} \tag{A5}$$

$$\Rightarrow \Delta V_I = -E\mathbf{I}^2(k)\sum_{i=1}^{5}\left(\hbar_I^i\left(\frac{\partial y_I}{\partial\chi_I^i}\right)^2\left(1 - \frac{1}{2}\hbar_I^i\left(\frac{\partial y_I}{\partial\chi_I^i}\right)^2\right)\right). \tag{A6}$$

Since $E\mathbf{I}^2 > 0$, the convergence is guaranteed if $\sum_{i=1}^{5}\left(\hbar_I^i\left(\frac{\partial y_I}{\partial\chi_I^i}\right)^2\left(1 - \frac{1}{2}\hbar_I^i\left(\frac{\partial y_I}{\partial\chi_I^i}\right)^2\right)\right) > 0$

$$\Rightarrow 2 - \hbar_I^i \max\left(\frac{\partial y_I}{\partial\chi_I^i}\right)^2 > 0 \tag{A7}$$

$$\Rightarrow 0 < \hbar_I^i < \frac{2}{\max\left(\frac{\partial y_I}{\partial\chi_I^i}\right)^2}. \tag{A8}$$

### Proof of Theorem 2:

For the control block, the change in Lyapunov function is given as:

$$\Delta V_C = V_C(k+1) - V_C(k) = \frac{1}{2}\left[E\mathbf{C}^2(k+1) - E\mathbf{C}^2(k)\right]. \tag{A9}$$

Proceeding in the same way as for identification block,

$$\Delta V_C = \Delta E\mathbf{C}(k)\left[E\mathbf{C}(k) + \frac{1}{2}\Delta E\mathbf{C}(k)\right]. \tag{A10}$$

Using Eq. (54) and $\Delta\chi_{C_i} = -\hbar_C^{i_i}\frac{\partial J\mathbf{C}}{\partial\chi_{C_i}} = \hbar_C^{i_i}E\mathbf{C}\left(k\right)\frac{\partial u}{\partial\chi_{C_i}}$ in Eq. (A10),

$$\Delta V_C = \left(\frac{\partial E\mathbf{C}\left(k\right)}{\partial\chi_C}\right)^T \hbar_C E\mathbf{C}(k)\frac{\partial u}{\partial\chi_C}\left\{E\mathbf{C}\left(k\right) + \frac{1}{2}\left(\frac{\partial E\mathbf{C}\left(k\right)}{\partial\chi_C}\right)^T \hbar_C E\mathbf{C}(k)\frac{\partial u}{\partial\chi_C}\right\}. \tag{A11}$$

$$Using Eq.(52), \frac{\partial E\mathbf{C}}{\partial\chi_C} = -\left[\left(\frac{\partial y}{\partial u}\right)^2 + \lambda\right]\frac{\partial u}{\partial\chi_C} \tag{A12}$$

$$\Rightarrow \Delta V_C = -\left(\left[\left(\frac{\partial y}{\partial u}\right)^2 + \lambda\right]\frac{\partial u}{\partial\chi_C}\right)^T \hbar_C E\mathbf{C}\left(k\right)\frac{\partial u}{\partial\chi_C}\left\{E\mathbf{C}\left(k\right) - \frac{1}{2}\left(\left[\left(\frac{\partial y}{\partial u}\right)^2 + \lambda\right]\frac{\partial u}{\partial\chi_C}\right)^T \hbar_C E\mathbf{C}\left(k\right)\frac{\partial u}{\partial\chi_C}\right\} \tag{A13}$$

$$\Rightarrow \Delta V_C = -E\mathbf{C}^2\left(k\right)\sum_{i=1}^{4}\left(\hbar_C^i\left[\left(\frac{\partial y}{\partial u}\right)^2 + \lambda\right]\left(\frac{\partial u}{\partial\chi_C^i}\right)^2\left(1 - \frac{1}{2}\hbar_C^i\left[\left(\frac{\partial y}{\partial u}\right)^2 + \lambda\right]\left(\frac{\partial u}{\partial\chi_C^i}\right)^2\right)\right). \tag{A14}$$

Since $E\mathbf{C}^2 > 0$, the convergence guaranteed if

$$\sum_{i=1}^{4}\left(\hbar_C^i\left[\left(\frac{\partial y}{\partial u}\right)^2 + \lambda\right]\left(\frac{\partial u}{\partial\chi_C^i}\right)^2\left(1 - \frac{1}{2}\hbar_C^i\left[\left(\frac{\partial y}{\partial u}\right)^2 + \lambda\right]\left(\frac{\partial u}{\partial\chi_C^i}\right)^2\right)\right) > 0$$

$$\Rightarrow 2 - \hbar_C^i\left[\left(\frac{\partial y}{\partial u}\right)^2 + \lambda\right]\left(\max\left(\frac{\partial u}{\partial\chi_C^i}\right)\right)^2 > 0 \tag{A15}$$

$$\Rightarrow 0 < \hbar_C^i < \frac{2}{\left[\left(\frac{\partial y}{\partial u}\right)^2 + \lambda\right]\left(\max\left(\frac{\partial u}{\partial\chi_C^i}\right)\right)^2}, \tag{A16}$$

which completes the proof.

## Nomenclature

| | |
|---|---|
| LFEMO | Low frequency electromechanical oscillations |
| SSSC | Static synchronous series Compensator |
| FACTS | Flexible AC transmission system |
| AVR | Automatic voltage regulator |
| PSS | Power system stabilizer |
| SISO | Single input, single output |
| MIMO | Multiple input, multiple output |
| SMIB | Single machine infinite bus |
| TSK | Takagi–Sugeno–Kang |
| PID | Proportional integral derivative |
| PLL | Phase-locked loop |
| PWM | Pulse width modulation |
| SPWVD | Smooth pseudo-Wigner–Ville Distribution |
| $\theta$ | Line current angle |
| $\phi$ | Firing angle |
| $m$ | Modulation index |
| $\psi_s$ | Converter output voltage angle |
| $v_{d\_inv}$ | d-axis converter output voltage |
| $v_{q\_inv}$ | q-axis converter output voltage |
| $R_{ss}$ | Series resistance of SSSC |
| $L_{ss}$ | Series inductance of SSSC |
| $C$ | Converter DC-side capacitance |
| $R_{DC}$ | Converter DC-side resistance |
| $v_{DC}$ | DC link capacitor voltage |
| $i_d$ | d-axis line current |
| $i_q$ | q- axis line current |
| $\Xi_\kappa$ | Set of disturbances applied to power system |
| $\varphi$ | Morlet wavelet function |
| $m_{ij}$ | $j$th membership function of $i$th input |
| $\chi_I$ | Update parameters' vector for identification block |

| | | | |
|---|---|---|---|
| $\chi_C$ | Update parameters' vector for control block | $\lambda$ | Momentum term |
| $\hbar$ | Learning rate | | |

## References


[1] Varma RK. Concepts of FACTS controllers. In: IEEE/PES Power Systems Conference and Exposition 2011; 20–23 March 2011; Phoenix, AZ, USA. Piscataway, NJ, USA: IEEE, pp. 1–6.

[2] Singh B. Applications of FACTS controllers in power systems for enhance the power system stability: a state-of-the-art. Int J Rev Comp 2011; 6: 40–69.

[3] Badar R, Khan L. Online adaptive NeuroFuzzy wavelet based SSSC control for damping power system oscillations. In: IEEE International Conference on Emerging Technologies (ICET-2012), 8–9 October 2012; Islamabad, Pakistan. Piscataway, NJ, USA: IEEE, pp. 1–6.

[4] Badar R, Khan L. Adaptive NeuroFuzzy Legendre based damping control paradigm for SSSC. In: 47th International Universities Power Engineering Conference (UPEC); 4–7 September 2012; London, UK. Piscataway, NJ, USA: IEEE, pp. 1–6, 2012.

[5] Badar R, Khan L. Nonlinear adaptive NeuroFuzzy wavelet based damping control paradigm for SSSC. Adv Electr Comput En 2012; 12: 97–104.

[6] Pal B, Chaudhuri B. Robust Control in Power Systems. New York, NY, USA: Springer, 2005.

[7] Eslami M, Shareef H, Mohamed A. Tuning of power system stabilizers using particle swarm optimization with passive congregation. Int J Phys Sci 2010; 17: 2658–2663.

[8] Eslami M, Shareef H, Mohamed A, Khajehzadeh M. Application of artificial intelligent techniques in PSS design: a survey of the state-of the-art methods. Prz Elektrotechniczn 2011; 87: 88–197.

[9] Eslami M, Shareef H, Mohamed A. Power system stabilizer design using hybrid multi-objective particle swarm optimization with chaotic. J Cent South Univ T 2011; 18: 1579–1588.

[10] Eslami M, Shareef H, Mohamed A, Khajehzadeh M. Damping of power system oscillations using genetic algorithm and particle swarm optimization. Int Rev Electr Eng-I 2010; 6: 2745–2753.

[11] Hingorani, NG. Flexible AC transmission. IEEE Spectrum 1993; 40–45.

[12] Hingorani NG, Gyugyi L. Understanding FACTS: Concepts and Technology of Flexible AC Transmission Systems. New York, NY, USA: IEEE Press, 1999.

[13] Mihalic R, Papic I. Static synchronous series compensator—a mean for dynamic power flow control in electric power systems. Electr Pow Syst Res 1998; 45: 65–72.

[14] Singh BN, Chandra A, Al-Haddad K, Singh B. Performance of sliding mode and fuzzy controllers for a static synchronous series compensator. IEE P-Gener Transm D 1999; 146: 200–206.

[15] Pillai GN, Ghosh A, Joshi A. Torsional interaction between an SSSC and a PSS in a series compensated power system. IEE P-Gener Transm D 2002; 149: 653–658.

[16] Zhang XP. Advanced modeling of the multi-control functional static synchronous series compensator (SSSC) in Newton power flow. IEEE T Power Syst 2003; 18: 1410–1416.

[17] Ngamroo I, Kongprawechnon W. A robust controller design of SSSC for stabilization of frequency oscillations in interconnected power systems. Electr Pow Syst Res 2003; 67: 161–176.

[18] Shakarami MR, Kazemi A. Evaluation of different options for SSSC-based stabilizer to improve damping inter-area oscillations in a multi-machine power system. Int Rev Electr Eng-I 2009; 4: 1336–1346.

[19] Haque MH. Use of SSSC to improve first swing stability limit and damping of a power system. Aust J Electr El Eng 2006; 3: 17–26.

[20] Al-Jowder F. Improvement of synchronizing power and damping power by means of SSSC and STATCOM. Electr Pow Syst Res 2007; 77: 1112–1117.

[21] Wang HF. Static synchronous series compensation to damp power system oscillations. Electr Pow Syst Res 2000; 54: 113–119.

[22] Kumkratug P, Haque MH. Improvement of stability region and damping of a power system by using SSSC. IEEE Power Eng Soc 2003; 3: 1417–1421.

[23] Swain SC, Mahapatra S, Panda S, Panda S. Design of DE optimized SSSC-based FACTS controller. Int J El Elect Eng 2012; 2: 12–27.

[24] Swain SC, Balirsingh AK, Mahapatra S, Panda S. Design of static synchronous series compensator based damping controller employing real coded genetic algorithm. Int J Electr El Eng 2011; 5: 180–188.

[25] Ajami A, Armaghan M. Application of multi-objective PSO algorithm for power system stability enhancement by means of SSSC. Int J Comput Electr Eng 2010; 2: 1793–8163.

[26] Qiao W, Harley RG, Venayagamoorthy GK. Fault-tolerant control for SSSC using neural networks and PSO. In: IEEE/PES Power Systems Conference and Exposition (PSCE); 29 October–1 November 2006; Atlanta, GA, USA. Piscataway, NJ, USA: IEEE, pp. 952–958.

[27] Panda S. Multi-objective evolutionary algorithm for SSSC based controller design. Electr Pow Syst Res 2009; 79: 937–944.

[28] Panda S. Modeling, simulation and optimal tuning of SSSC based controller in a multi-machine power system. World J Model Sim 2010; 6: 110–121.

[29] Panda S, Padhy NP, Patel RN. Power-system stability improvement by PSO optimized SSSC-based damping controller. Electr Pow Compo Sys 2008; 36: 468–490.

[30] Panda S, Swain SC, Rautray PK. Design and analysis of SSSC-based damping controller. Simul Model Pract Th 2010; 18: 1199–1213.

[31] Abdelazim T, Malik OP. Adaptive fuzzy control of SSSC to improve damping of power system oscillations. In: IEEE Power Engineering Society General Meeting 2006; Montreal, Quebec, Canada. Piscataway, NJ, USA: IEEE.

[32] Singh B, Sharma NK, Tiwari AN. Classification of coordinated control techniques of FACTS controllers in emerging power systems: a review. Int J Sci T 2010; 1: 18–34.

[33] Murali D, Rajaram M. Intelligent control schemes for SSSC based damping controllers in multi-machine power systems. Int J Eng Sci T 2010; 2: 3788–3796.

[34] Murali D, Rajaram M. Power system damping using neuro-fuzzy based static synchronous series compensator controllers. Eur J Sci Res 2011; 60: 49–158.

[35] Murali D, Rajaram M, Reka N. Comparison of FACTS devices for power system stability enhancement. Int J Comput Appl 2010; 8: 30–35.

[36] Chandrakar VK, Kothari AG. Fuzzy logic based static synchronous series compensator (SSSC) for transient stability improvement. In: IEEE International Conference on Electric Utility Deregulation, Restructuring and Power Technologies; 5–8 April 2004; Hong Kong, China. Piscataway, NJ, USA: IEEE, pp. 240–245.

[37] Abiyev RH. Controller based on fuzzy wavelet neural network for control of technological processes. In: IEEE International CISMA; 20–22 July 2005; Giardini, Naxos, Italy. Piscataway, NJ, USA: IEEE, pp. 215–219.

[38] Abiyev RH. Time series prediction using fuzzy wavelet neural network model. Lect Notes Comput Sc 2006; 191–200.

[39] Wang CH, Wang WY, Lee TT, Tseng PS. Fuzzy B-spline membership function and its applications in fuzzy-neural control. IEEE T Syst Man Cybe 1995; 25: 841–851.

[40] Abe S. Dynamic cluster generation for a fuzzy classifier with ellipsoidal regions. IEEE T Syst Man Cybe Part-B 1998; 28: 869–876.

[41] Mohaghegi S, Venayagamoorthy GK, Harley RG. Fully evolvable optimal neurofuzzy controller using adaptive critic designs. IEEE T Fuzzy Syst 2007; 16: 1450–1461.

[42] Sala A, Guerra TM. Stability analysis of fuzzy systems: membership shapes and polynomial approaches. In: 17th World Congress International Federation of Automatic Control; 6–11 July 2008; Seoul, Korea. Seoul: International Federation of Automatic Control, pp. 5605–5610.

[43] Abiyev RH, Kaynak O. Type 2 fuzzy neural structure for identification and control of time-varying plants. IEEE T Indus Elect 2010; 57: 4147–4158.

[44] Curry HB, Schoenberg IJ. On Pólya frequency functions IV: The fundamental spline functions and their limits. J Anal Math 1966; 17: 71–107.

[45] Zhang J, Le KV, Knoll A. Unsupervised learning of control surfaces based on B-spline models. In: 6th IEEE International Conference on Fuzzy Systems; 1–5 July 1997; Barcelona, Spain. New York, NY, USA: IEEE, pp. 1725–1730.

[46] Wang WY, Lee TT, Leu CL, Wang CH. Function approximation using fuzzy neural networks with robust learning algorithm. IEEE T Syst Man Cy B 1997; 27: 740–747.

[47] Wu ZQ, Harris CJ. A neurofuzzy network structure for modeling and state estimation of unknown nonlinear systems. Int J Syst Sci 1997; 28: 335–345.

[48] Wang K, Lei B. Using B-spline neural network to extract fuzzy rules for a centrifugal pump monitoring. J Intel Manuf 2001; 12: 5–11.

[49] Leu YG, Wang WY, Lee TT. Robust adaptive fuzzy-neural controllers for uncertain nonlinear systems. IEEE T Robotic Autom 1999; 15: 805–817.

[50] Padiyar KR. Power System Dynamics Stability and Control. Hyderabad, India: B.S. Publications, 2000.

[51] Torii M, Hagan MT. Stability of steepest descent with momentum for quadratic functions. IEEE T Neural Network 2002; 13: 752–756.

[52] Liu Z. Self-tuning control of electrical machines using gradient descent optimization. Optim Contr Appl Met 2006; 28: 77–93.

[53] Lee CH, Teng CC. Identification and control of dynamic systems using recurrent fuzzy neural networks. IEEE T Fuzzy Syst 2000; 8: 349–366.

[54] Kunder P. Power System Stability and Control. New York, NY, USA: McGraw-Hill Inc., 2008.

[55] Romera EG, Jaramillo MA, Fernandez DC. Monthly electric energy demand forecasting with neural networks and Fourier series. Energ Convers Manage 2008; 49: 3135–3142.

[56] Bradford SC. Time-frequency analysis of systems with changing dynamic properties. PhD, California Institute of Technology, Pasadena, California, 2006.